ELSEVIER

Remote Sensing of Environment 80 (2002) 297–307

Remote Sensing of Environment

www.elsevier.com/locate/rse

Sensitivity of multitemporal NOAA AVHRR data of an urbanizing region to land-use/land-cover changes and misregistration

Douglas A. Stow*, Dong Mei Chen

Department of Geography, San Diego State University, San Diego, CA 92182-4493, USA

Received 25 January 2001; received in revised form 13 August 2001; accepted 21 August 2001

Abstract

Our objectives were to: (1) investigate the sensitivity of multitemporal image data from the Advanced Very High Resolution Radiometer (AVHRR) satellite data for detecting land-use/land-cover changes primarily associated with urbanization and (2) test the effectiveness of a misregistration compensation model on the same data set. Empirical analyses were conducted using two near-anniversary, single-date NOAA AVHHR images of a rapidly urbanizing region of southern and Baja California. Analyses were facilitated by reference data from detailed GIS data layers of land-use/land-cover types for the 2 years corresponding to image acquisition dates (1990 and 1995). Almost all AVHRR pixels containing land-use/land-cover changes were mixed with nonchange areas, even when the extent of change features was greater than the nominal 1 km^2 ground sampling area. The strongest signals of image brightness change were detected by temporal differences of NDVI and Channel 4 surface temperature. ''Undeveloped to urban'' and ''undeveloped to water'' were the land-use/land-cover transition sequences with the most definitive AVHRR change signals. Mean magnitudes of misregistration errors were estimated to be around 0.2 pixel units in x and y directions. Mean values for misregistration noise equivalent in brightness change (MNEΔB) were 0.02, 0.02, and 1.96 K for image differences of Channel 1 reflectance, NDVI, and Channel 4 surface temperature, respectively. The misregistration compensation model reduced false detection of change, but improvements in detection of land-use/land-cover changes were not conclusive.

1. Introduction

A recent emphasis of the interdisciplinary field of earth system science is the acknowledgment of the importance of land-use/land-cover changes in influencing and signaling global and environmental change (Vitousek 1994). Some changes in land use and land cover result from natural disturbance mechanisms, while others have anthropogenic causes (Douglas, 1994). Human activities directly (e.g., urban development as a change in land use) and indirectly (e.g., alteration of fire or moisture regimes) cause land-use/land-cover changes (Turner, Meyer, & Skole, 1994). Conversely, land-use/land-cover changes have direct and indirect effects on earth systems, such as the hydrologic and carbon cycles (Penner, 1994).

The only feasible means for comprehensive land-cover monitoring of the entire terrestrial surface of the Earth is by remote sensing with satellite imaging systems. In spite of advances in digital imaging, transmission, computing, and storage capabilities at the beginning of the 21st century, continental- to global-scale monitoring of land-use/land-cover change is necessarily limited to sensors with moderate to coarse spatial resolution operating on polar orbiting satellites (Turner et al., 1994). The Advanced Very High Resolution Radiometer (AVHRR) on the National Oceanic Atmospheric Administration (NOAA) series of satellites has been the mainstay for continental-to global-scale monitoring (Malingreau, 1986; Schultz & Halpert, 1995). Having a nominal 1.1-km spatial resolution at nadir and a nominal swath of coverage of 2700 km, the system has provided global daily coverage at full resolution in an operational manner since the early 1980s. By screening clouds and/or maximum value compositing (Eidenshink, 1992), changes in land use and land cover can be feasibly tracked for time scales varying from a months to 15 years. Similar, newer generation sensors such as Vegetation on the

* Corresponding author. Tel.: +1-619-594-5498; fax: +1-619-594-4938.

E-mail address: stow@mail.sdsu.edu (D.A. Stow).

0034-4257/01/$ – see front matter
PII: S0034-4257(01)00311-X

SPOT-4 satellite enable more cloud-free imaging opportunities per day and an additional waveband in the shortwave infrared part of the spectrum. The Moderate Resolution Imaging Spectrometer (MODIS) on the TERRA satellite provides a new generation of global land-use/land-cover change products.

Yet to be fully understood is the sensitivity of multitemporal AVHRR data for capturing land-use/land-cover changes of interest, particularly those associated with human activities (Lambin, 1997; Mucher, Steinnnocher, Kressler, & Heunks, 2000). Neither are the impacts of noise sources such as misregistration on detecting detailed changes well known. Relative to the sizes of most anthropogenic land-use/land-cover changes, AHVRR data are best characterized by the low or L-resolution scene model of Strahler, Woodcock, and Smith (1986). That is, most changes in land use and land cover are smaller than the ground sampling distance (GSD) of the AVHRR sensor (Cherchali, Amram, & Flouzat, 2000; Foody & Boyd, 1999). While surface features that are smaller than the GSD and are highly contrasting relative to background elements can be detected and even measured (Dozier, 1981; Hope, Coulter, & Stow, 1999), noise can obscure signals of smaller extent or weaker contrast. Noise sources include radiometric influences such as drift in sensor calibration, variability in atmospheric optical properties, and changes in illumination conditions. Other noise sources pertain to geometric effects, of which misregistration (i.e., errors in co-alignment of multiple images) is the most significant (Carmel, Dean, & Flather, 2001; Coppin & Bauer, 1996; Dai & Khorram, 1998; Roy, 2000). A key to successful detection or measurement of land cover changes then is to minimize noise effects through careful selection of imagery and successful application of image processing techniques.

The objectives of the research reported in this paper were to:

1. investigate the sensitivity of multitemporal NOAA AVHRR imagery for detecting land-use/land-cover changes that are mostly subpixel in extent and primarily associated with human activities and
2. test a model that compensates for misregistration within a multitemporal NOAA AVHRR data set and determine if the sensitivity of detecting land-use/land-cover change signals is enhanced.

Both objectives were met through an empirical assessment based on reliable reference data.

2. Background

Most studies of the utility of AVHRR for monitoring land-use/land-cover changes have emphasized regional to continental-scale changes in vegetation greenness over seasonal/phenological cycles, and interannual differences in vegetation phenology and vigor as a result of climatic variability (Bastin, Pickup, & Pearce, 1995; Nicholson, Tucker, & Ba, 1998; Tucker, Dregne, & Newcomb, 1991). Townshend, Justice, Gurney, and McManus (1992) identified the following transitions as some of the primary anthropogenic signals that are thought to be detectable with some degree of certainty using AVHRR and other moderate- to coarse-resolution optical satellite system: (1) agricultural encroachment on rangeland, (2) intensification of rangeland use, (3) conversion of natural vegetation to rangeland or agriculture, and (4) loss and regrowth of vegetation from logging and fire. None of these transitions include land-use/land-cover change associated with expansion of intensive settlements (i.e., urbanization).

Misregistration of multitemporal imagery may be the most significant source of noise when monitoring land-use/land-cover changes with moderate-to coarse-resolution sensors such as MODIS and AVHRR (Townshend et al., 1992). Using simulated MODIS data, Townshend et al. (1992) reported that artifacts from image differencing of misregistered spectral vegetation index (SVI) values are likely to be more prevalent than SVI difference values from actual land-use/land-cover changes. They also found that the misregistration effects on image differencing were greatest for multitemporal data sets of regions with pixels that were spatially heterogeneous.

As introduced in Stow (1999), a simple model of the factors influencing the magnitude of pixel based image differencing is:

$$\frac{\Delta B}{\Delta t} = -\frac{\Delta B}{\Delta x} D_x - \frac{\Delta B}{\Delta y} D_y + R + S \tag{1}$$

where B is the image brightness (i.e., digital number, radiance, reflectance, surface temperature) value; $(\Delta B/\Delta t)$ is the discrete temporal change in image brightness (B) over time interval Δt, i.e., image difference; $(\Delta B/\Delta x)$ and $(\Delta B/\Delta y)$ are the discrete spatial gradients of image brightness in the x (east–west) and y (north–south) directions, respectively; D_x and D_y are misregistration magnitudes in x and y directions, respectively; R is the temporal difference in B due to radiometric inconsistencies (e.g., sensor noise, sensor calibration drift, and differences in illumination and atmospheric optical properties); and S is the temporal change in B resulting from actual land surface changes, i.e., the signal. Note that image brightness (B) represents the generic term for the pixel magnitude and should not be confused with "brightness" from the tasseled-cap transform or the antenna brightness for passive microwave radiometry.

When Eq. (1) is rearranged, the change signal term (S) is isolated to yield:

$$S = \frac{\Delta B}{\Delta t} + \frac{\Delta B}{\Delta x} D_x + \frac{\Delta B}{\Delta y} D_y - R \tag{2}$$

Eq. (2) shows that land-use/land-cover change signals can be retrieved with greater accuracy from the temporal brightness change if the magnitude of misregistration and spatial gradients of brightness can be estimated reliably and radiometric attributes can be minimized through multitemporal normalization. Assumptions and approaches to estimating the magnitude of misregistration, and numerical methods for solving Eq. (2) are presented in Stow (1999).

3. Study area

An extensive study area was selected covering a 404,000-km^2 region that encompasses a large portion of southern California, southwestern Arizona, and the upper portion of Baja California, Mexico. The delineation of the study area was based on the extent of mostly cloud free coverage of the two multitemporal NOAA AVHRR image subsets that were selected for analysis of the 1990–1995 study period (Fig. 1). The extensive study area has semiarid or arid climates and the natural vegetation cover consists of Mediterranean-type shrublands and forests, and deserts, with small (relative to the AHVRR spatial resolution) extents of grasslands, riparian forests, and coastal wetlands. Topography and physiography are diverse. Urban developments of the large metropolis within Los Angeles, Orange, San Bernadino and Riverside Counties, and the San Diego–Tijuana urban complex are the dominant land-use features of the extensive study area.

An intensive study area covering San Diego County, CA (excluding the Camp Pendleton military base) was selected for the bulk of the analyses. This area was selected because of the availability of reliable land-use and vegetation (land-cover) GIS data layers for the years 1990 and 1995. Most of the variability of climate, vegetation, topography, physiography, and land use within the extensive study area is found within San Diego County.

4. Data and methods

4.1. Overview

Multitemporal NOAA AVHRR data captured on near-anniversary dates were geometrically and radiometrically processed and then subjected to standard change detection routines. Extant land-use/land-cover GIS layers in vector format for the years corresponding to the multitemporal AVHRR data were obtained as reference data. A misregistration compensation model was applied, utilizing residuals of ground control points (GCPs) to determine relative magnitude of misregistration. Sensitivity of detecting specific sizes and types of land-use/land-cover change features was examined by comparing AVHRR-derived products (with and without the misregistration compensation model) to the reference data. The utility of the miregistration compensation model was also assessed through spatial statistical analyses.

4.2. NOAA AVHRR data acquisition and preprocessing

Two NOAA AVHRR Local Area Coverage (LAC) images extracted from orbital segments were obtained from the United States Geological Survey (USGS) Earth Resources Observation System (EROS) Data Center (EDC); a NOAA-11 image captured at 21:41 GMT on 14 June 1990

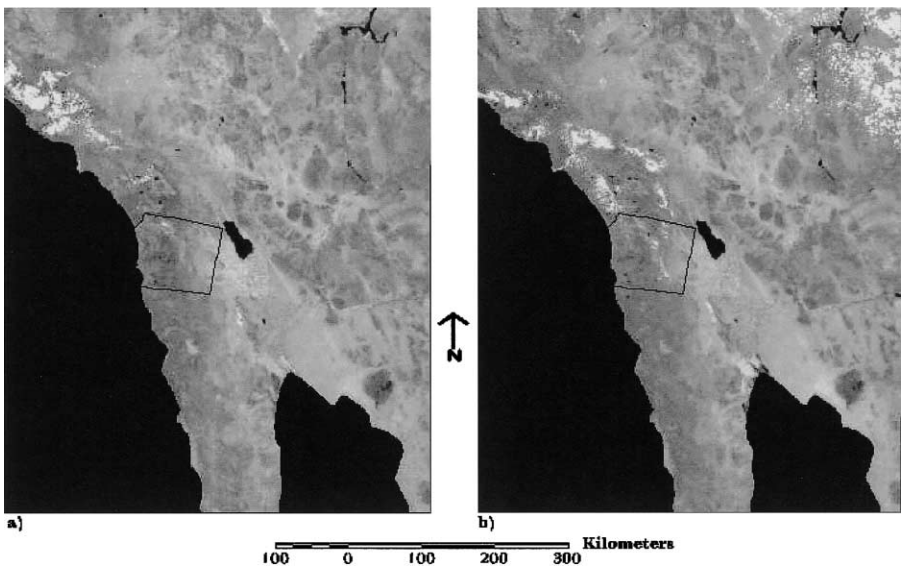

Fig. 1. NOAA AVHRR image subsets of southwestern US. Polygon delineates intensive study area covering most of San Diego County, CA. (a) 14 June 1990 and (b) 17 June 1995.

and a NOAA-14 image at 21:16 GMT on 17 June 1995. The AVHRR image data had been subjected to standard AVHRR Data Acquisition and Processing System (ADAPS) geometric and radiometric processing by EDC. This includes geometric rectification, georeferencing to the Lambert Azimuth Equal-area coordinate system, radiometric calibration, and conversion to spectral reflectance factors for Channels 1 (visible red) and 2 (near infrared) and apparent radiometric temperatures for Channels 3, 4, and 5 (thermal infrared). A library of GCPs is used in the ADAPS rectification and georeferencing process, which is partially achieved by means of registration to a georeferenced image base. We made a special request to the EDC to obtain data on residual errors for GCPs that were used in the ADAPS processing to register the two AVHRR image segments. The residuals represent the differences or offsets between the positions of the image base GCPs and those predicted by the geometric transformation model, for each image that is registered to that base. Subsets from the near-nadir viewing portions of the two image segments covering a common area (as described above) were extracted for subsequent processing and analysis.

Other than the radiometric calibration and normalization procedures implemented as part of ADAPS processing, no other radiometric processing was implemented (e.g., scene-based normalization or atmospheric correction). The between-date radiometric bias is minimal and can be inferred from Table 1.

4.3. Estimation of misregistration surfaces

Misregistration surfaces or images, depicting apparent errors of co-alignment in two (horizontal) dimensions between two registered images, were estimated from the residuals of the GCPs generated from the original ADAPS registration procedures. The x and y misregistration surfaces are required inputs to the misregistration compensation model. Since the two AVHRR segments were registered independently to the same image control base, their co-registration is implicit. A total of 35 GCPs within the extensive study area had been used in ADAPS processing of the 1990 image and 31 for the 1995 image. Of these GCPs, 26 were common between both dates. GCP residual values for each date were surfaced using an interpolation routine in ERDAS Imagine image processing software, yielding a raster image of apparent registration errors having 1-km pixels. The x and y error surfaces from the 1990 image were subtracted from the 1995 error surfaces to create the misregistration surfaces.

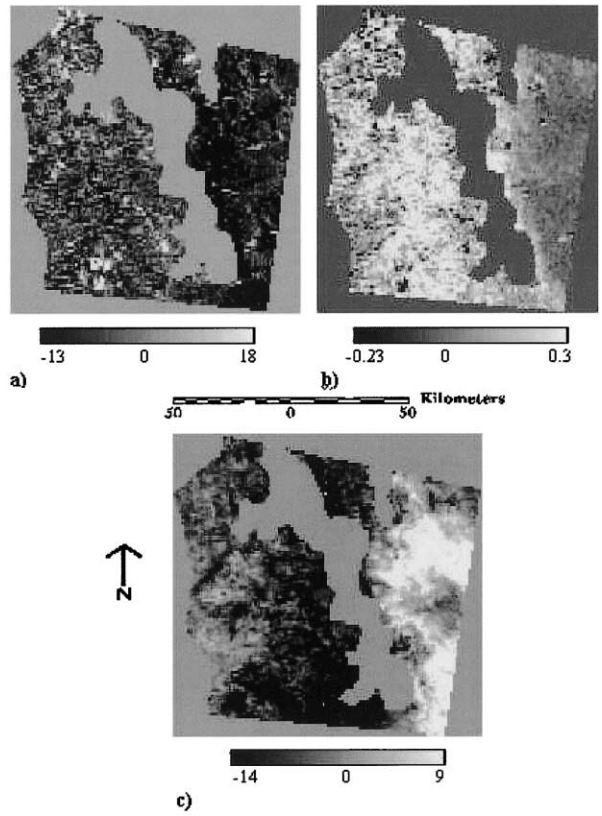

Fig. 2. Difference images for intensive study area derived from (a) Channel 1 (visible) reflectance factors, (b) NDVI, and (c) Channel 4 (TIR) radiometric temperature values. Cloud, ocean, and study area mask represented as medium grey tone.

Table 1
Statistics for AVHRR image derivatives of extensive study area (excluding ocean and clouds)

Image derivative	Minimum	Maximum	Mean	S.D.
1990 Ch1 reflectance	0.04	0.58	0.26	0.06
1995 Ch1 reflectance	0.03	0.60	0.23	0.05
ΔCh1 reflectance	− 0.32	0.27	− 0.03	0.02
1990 NDVI	− 0.050	0.56	0.08	0.07
1995 NDVI	− 0.050	0.56	0.08	0.07
ΔNDVI	− 0.63	0.59	0.12	0.08
1990 Ch4 temperature	294 K	327 K	316 K	5 K
1995 Ch4 temperature	288 K	324 K	314 K	5 K
ΔCh4 temperature	− 24 K	12 K	− 2 K	3 K

Δ = 1995 − 1990.

4.4. Image differencing

Simple image differencing was performed using the standard multitemporal difference formula:

$$\frac{\Delta B}{\Delta t} = (B_i^{t=2} - B_i^{t=1}) \quad (3)$$

where $t=2$ and $t=1$ are the later and earlier (i.e., master or base) images, respectively, and i denotes the pixel of operation.

Multitemporal differences were calculated for three channels or derivative inputs from the 1990 and 1995 AHVRR images: (1) Channel 1 (Ch1) reflectance, (2) normalized difference vegetation index (NDVI), and (3) surface

temperature derived from Channel 4 (Ch4) radiance (Fig. 2). Ch1 differences primarily represent changes in surface albedo between image dates. NDVI, derived as (Eq. (4)):

$$\mathrm{NDVI} = (R_{\mathrm{Ch2}} - R_{\mathrm{Ch1}})/(R_{\mathrm{Ch2}} + R_{\mathrm{Ch1}}) \quad (4)$$

using spectral reflectance factors (R_λ) was differenced as an indicator of change in vegetation greenness. Image differencing of radiometric temperatures derived from Ch4 radiances was shown by Lambin and Strahler (1994) to emphasize changes in landscape moisture, potentially as a result of land-use/land-cover changes.

4.5. Misregistration compensation model

To compensate for misregistration effects on image differencing, a numerical model based on a simplification of Eq. (2) was applied, in attempt to isolate image differences resulting from land-use/land-cover changes (Stow, 1999). Temporal differences were derived in the same manner as standard multitemporal image differencing (Eq. (3)). A directional, first-order gradient operator was utilized to estimate horizontal gradients in the N–S and E–W directions (Eqs. (5a) and (5b)), rather than using the central difference gradient method tested by Stow (1999):

$$\frac{\Delta B}{\Delta x} \text{ or } \frac{\Delta B}{\Delta y} = (B_{i+l}^{t=2} - B_i^{t=2}) \text{ for } D_x \text{ or } D_y \geq 0 \quad (5a)$$

or

$$\frac{\Delta B}{\Delta x} \text{ or } \frac{\Delta B}{\Delta y} < 0 = (B_i^{t=2} - B_{i-l}^{t=2}) \text{ for } D_x \text{ or } D_y < 0. \quad (5b)$$

where i is incremented along rows for the x gradient and along columns for the y gradient, and $i+1$ is the pixel ahead and $i-1$ is the pixel behind the pixel of operation.

4.6. Reference data

Existing GIS and imagery data sets were acquired from on-line databases of the San Diego Association of Governments and refined to serve as reference data for assessing the types and characteristic sizes of land-use/land-cover changes detected with the multitemporal AVHRR data set. The data sets cover the entirety of San Diego County, an area slightly greater than 10,000 km^2. Analyses of sensitivity and validation of the AVHRR-derived change detection products were limited to this area.

The most useful of the reference data sets were GIS layers portraying land use for 1990 and 1995. These land-use layers had been derived by SANDAG using on-screen interpretation and digitizing of orthorectified SPOT panchromatic (Pan) and multispectral (XS) imagery, aided by aerial photographs and field reconnaissance. Land-use polygons were classified as one of 19 categories, including a broad category called "vacant and undeveloped." Where evident, artifacts from misregistration, classification errors, and inconsistencies in classification schemes of the 1990 and 1995 layers were edited. Other GIS layers used to validate the AVHRR change products portray vegetation and land-cover types for 1990 and 1995, which had been mapped within the "vacant and undeveloped" polygons of the land-use layers. Almost all of the changes evident between the 1990 and 1995 vegetation layers represent land-use change (e.g., transition from "vacant and undeveloped" to "developed") and few land-cover changes (e.g., vegetation type changes or wildfires) were evident. After merging land-use and land-cover data, the final validation product was a digital map depicting percentage land-use/land-cover change per square kilometer pixel.

5. Results

5.1. Land-use/land-cover changes and their signals

Statistics for single date and image difference images for each of the three AVHRR derivatives (Ch1 reflectance factor, NDVI, and Ch4 surface temperature) of the extensive study area (excluding ocean and clouds) are listed in Table 1. The mean image difference values, 0.19, 0.02, and 1.96 K, respectively, indicate the temporal bias between dates. Some of the bias is due to incomplete radiometric normalization (particularly from atmospheric effects) and

Table 2
Characteristics of land-use/land-cover change features[a]

Transition type (from–to)	No. of features	Mean size (km^2)	Mean (ΔCH1)	Mean (ΔNDVI)	Mean (ΔCh4)	No. of pixels
1. Agriculture to urban	2	0.69	−1.333	0.045	−8	3
2. Agriculture to undeveloped	5	1.036	−1.625	0.0817	−3.5	8
3. Under construction to urban	3	0.61	−5.25	0.149	−3.5	4
4. Undeveloped to agriculture	9	2.212	−3.3077	0.087	−4	25
5. Undeveloped to under construction	3	0.86	1	−0.015	−1.714	4
6. Undeveloped to urban	8	1.519	−3.0625	0.116	−4.562	16
7. Undeveloped to water	5	2.168	−3.642	0.0034	−11.5	15

Δ = 1995 – 1990.

[a] Features greater than 0.5 km^2 and percentage of land-use change greater than 50%.

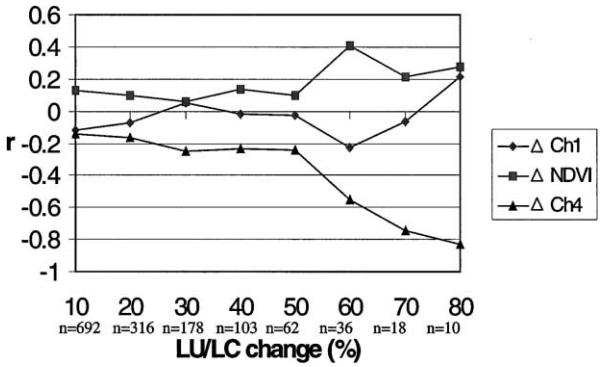

Fig. 3. Correlation coefficients (r) for image difference value vs. percentage of land-use/land-cover change for Channel 1 (visible) reflectance, NDVI, and Channel 4 (TIR) radiometric temperature images. Higher correlation coefficients signify greater sensitivity to land-use/land-cover changes. Correlation coefficients were not statistically significant until the areal extent of land-use/land-cover change features was at least 70% of the extent of an AVHRR pixel.

some due to differences in surface conditions at the time and date of imaging. The latter influence is particularly noticeable by higher NDVI values for 1995 in the chaparral-dominated undeveloped areas of southern California and the higher Ch4 surface temperatures of the Mojave and Sonoran Deserts.

Seven general sequences or transitions of land-use/land-cover change were identified from the detailed reference data of the San Diego County study area and are listed in Table 2. In all, there were 35 change features (i.e., polygons) between 1990 and 1995 that were at least 0.5 km^2 in extent. Roughly half of these features were at least 1 km^2 in size (i.e., the nominal spatial resolution of the AVHRR data).

The initial (1990) states of the transition (“from–to”) sequences for specific change features were either “agriculture,” “under construction,” or “undeveloped” land-use types. Most of the change features that were “undeveloped” in 1990 consisted of natural vegetation and bare ground land-cover types. A majority of the change features transitioned to “agriculture,” “under construction,” “urban,” and “water.” The largest and most commonly occurring transition types were “undeveloped to agriculture,” 21% overall and 24% of features greater than 0.5 km^2, and “undeveloped to urban,” 20% overall and 21% of features greater than 0.5 km^2.

The sign and magnitude of AVHRR signals of land-use/land-cover changes for Ch1, NDVI and Ch4 are also shown in Table 2. Signals are characterized by the mean multitemporal differences derived from all pixels containing at least 50% change of a single transition sequence. Given the relatively small number of pixels meeting this criterion, few clear signals of change are evident, particularly when factoring in the radiometric bias between images. Of the seven transition sequences observed, only “undeveloped to agriculture,” “undeveloped to urban,” and “undeveloped to water” were represented by a sufficient number of AVHRR pixels meeting the 50% or more change criterion. Only the latter two transition types showed significant departures from the apparent radiometric bias, primarily in the NDVI and Ch4 difference images. The “undeveloped to urban” exhibited a moderate increase in NDVI and moderate decrease in Ch1 reflectance and Ch4 temperature, while “undeveloped to water” showed a small decrease in NDVI and large decrease in Ch4 temperature. The “under construction to urban” transition was represented by a small sample of pixels, but appears to exhibit detectable signals in all three difference images.

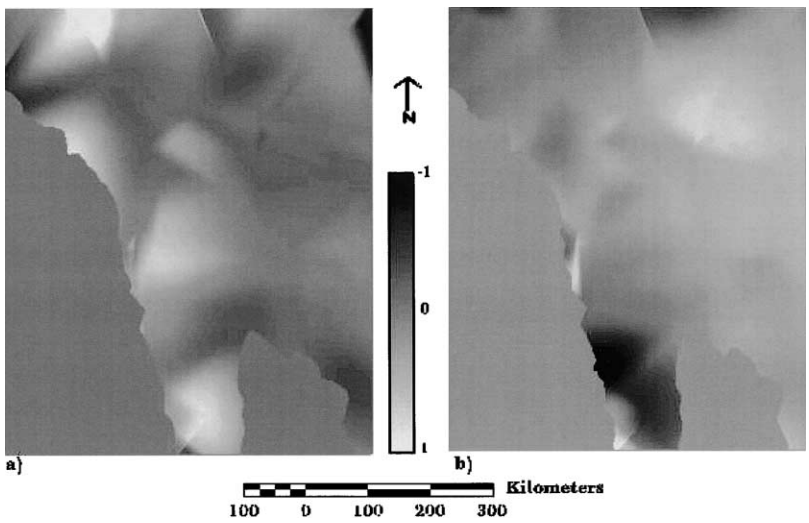

Fig. 4. Misregistration fields (images) of extensive study area depicting magnitude and sign of apparent misregistration in the (a) x and (b) y directions. Derived by surfacing the residuals of ground control points for each image date and differencing the residual surfaces.

Table 3
Magnitudes of estimated misregistration errors

Misregistration	Minimum	Maximum	Mean	S.D.
D_x	0.00	0.95	0.23	0.21
D_y	0.00	0.97	0.18	0.20
D_h	0.00	1.24	0.33	0.25

5.2. Sensitivity to land-use/land-cover change

Sensitivity of image difference products was tested by spatial comparisons with percentage change maps derived from reference data portraying land-use/land-cover change for 1990–1995. This was achieved by spatial overlay and cross-tabulation of the difference image magnitudes with the percentage change maps. Pixels were progressively screened at increasing intervals of 10% land-use change per square kilometer (i.e., AVHRR pixel) and correlation coefficients were calculated after each screening. This screening was discontinued at the 80% change level, as the number of 1-km pixels having this amount of change dropped to 10.

Correlation of percentage land-use/land-cover change in relation to each of the AVHRR difference maps is graphed in Fig. 3. Correlation coefficients were not significant for any of the difference maps until the 60% land-use/land-cover change level was reached. Significant correlations occurred at this level for both NDVI and Ch4 temperature difference images. No significant correlations or visual correspondence with the reference data were evident for Ch1 differences, even when examining pixels with high proportions of changes.

5.3. Misregistration effects

The density of GCPs from the ADAPS library is low (for the study area), such that the misregistration fields were derived by interpolation of a sparse distribution of points. On average for the terrestrial area of the extensive AVHRR subset, the density of GCPs was one point per 8800 km^2. For the most part, the misregistration fields were smoothly varying and abrupt changes in magnitude and sign of errors at proximal GCPs were limited.

As estimated by the x and y misregistration fields of the extensive study area subset, magnitudes of apparent co-location errors between the two dates of AVHRR imagery were less than one pixel in both dimensions (Fig. 4). Statistics for the magnitudes of the misregistration error are listed in Table 3. These magnitudes imply that the ADAPS registration was reasonably precise and that errors in registration are "subpixel" in magnitude. The mean value of the total (x and y) misregistration error (D_h) is 0.33 pixel units or approximately 0.33 km.where:

$$D_h = (D_x^2 + D_y^2)^{1/2}.$$

Fig. 5 portrays the magnitudes of the apparent horizontal misregistration (D_h) error derived from the misregistration fields of the extensive study area for the 1990–1995 image pair relative to the spatial brightness gradient ($\Delta B/\Delta h$) of the 1995 (i.e., most recently acquired) image. The scatterplots for each of the three band difference images are based on all pixels within the extensive study area. All three scatterplots have similar form, with the median and mode of D_h occuring at around 0.2 pixel units.

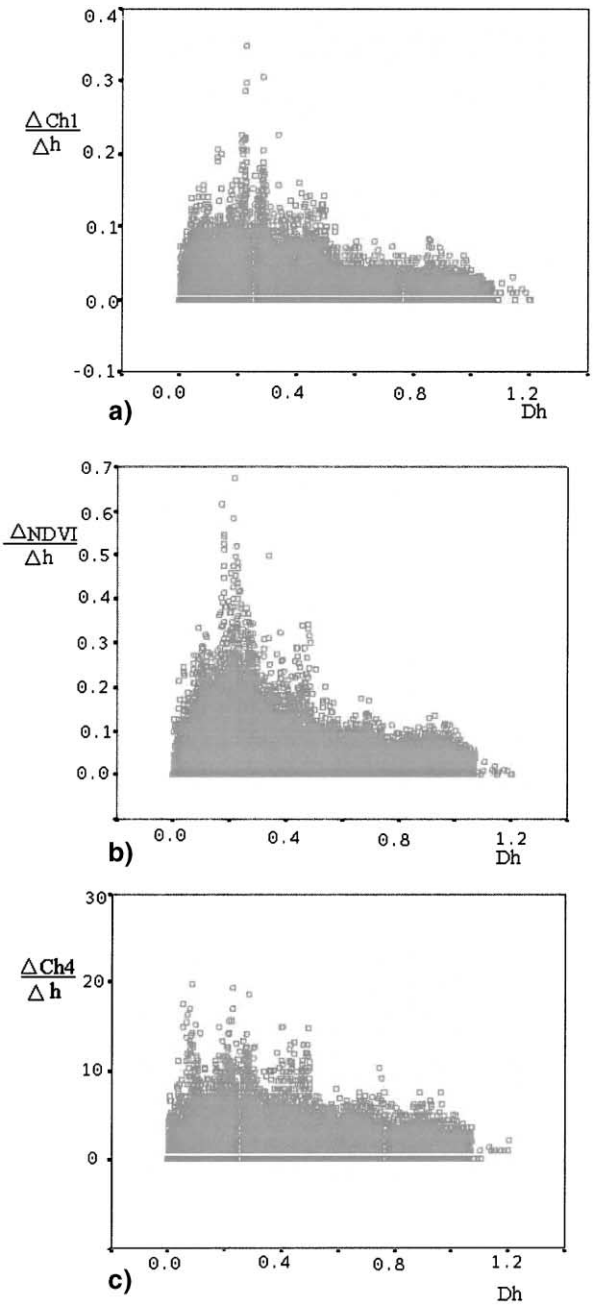

Fig. 5. Scatterplots depicting spatial brightness gradient ($\Delta B/\Delta h$) vs. horizontal misregistration (D_h) for 1995 AVHRR pixels within extensive study area for (a) ΔCh1, (b) ΔNDVI, and (c) ΔCh4.

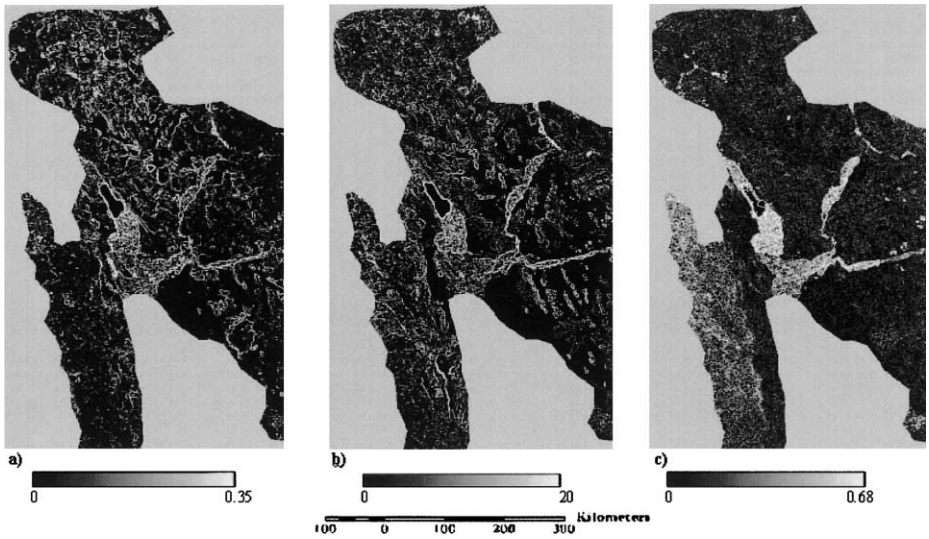

Fig. 6. Images portraying the magnitude of MNEΔB for (a) ΔCh1, (b) ΔNDVI, and (c) ΔCh4.

The combined effect of the horizontal misregistration (D_h) error times the spatial brightness gradient ($\Delta B/\Delta h$) quantifies the effect of misregistration on the image difference calculation. The misregistration noise equivalent difference in brightness (MNEΔB) can be estimated as:

$$\mathrm{MNED}B = \left(D_h * \frac{\Delta B}{\Delta h}\right)$$

where:

$$\frac{\Delta B}{\Delta h} = \left(\left(\frac{\Delta B}{\Delta x}\right)^2 + \left(\frac{\Delta B}{\Delta y}\right)^2\right)^{1/2}$$

Images of the magnitude of MNEΔB for all three image difference bands are shown in Fig. 6 and statistics are listed in Table 4.

The MNEΔB statistics and images for ΔCh1, ΔNDVI, and ΔCh4 show that the influence of misregistration error on image difference calculations can be locally substantial, even when the misregistration errors are minimal. The images of MNEΔB show that there is little coherent pattern to misregistration noise for this specific AVHRR data set. Many of the higher magnitude pixels occur at the edges and within the irrigated agricultural lands of Imperial and Coachella Valleys. The relatively large agricultural fields with varying crop types and phenological stages result in large values of ($\Delta B/\Delta h$), particular for NDVI and Ch4 temperature.

Table 4
Magnitudes of misregistration noise equivalent difference in brightness (MNEΔB) for ΔCh1, ΔNDVI, and ΔCh4

MNEΔB	Minimum	Maximum	Mean	S.D.
ΔCh1	0.00	0.35	0.02	0.01
ΔNDVI	0.00	0.67	0.02	0.03
ΔCh4	0.00 K	19.85 K	1.96 K	1.18 K

Δ = 1995 – 1990.

5.4. Misregistration compensation model

To assess the utility of the misregistration compensation model, the same spatial correlation tests applied to the simple band difference images were run using AVHRR difference products generated by the model. Correlation coefficients for the model products of the intensive study area relative to the reference map of percentage change are shown in Fig. 7. These correlation coefficients were derived in the same manner as those for simple image difference products (Fig. 3) and are not significantly different. This result suggests that the compensation model provided no significant improvement in detecting land-use/land-cover change features.

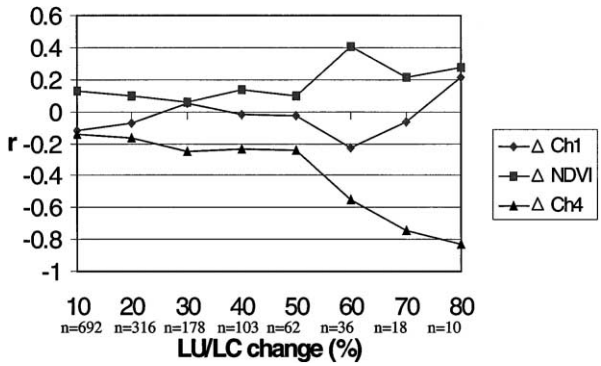

Fig. 7. Correlation coefficients (r) for output of misregistration compensation model relative to the reference map of percentage change. Similar plot as for output of simple image differencing shown in Fig. 3 (above).

Global variance values for the products generated from the misregistration compensation model for the extensive study area are nearly identical for ΔCh1, significantly lower for ΔNDVI, and significantly higher for ΔCh4 than those for each of the corresponding simple band difference images. This suggests that the model was most effective in reducing the effects of misregistration noise for ΔNDVI and created more artifacts than reduced noise for ΔCh4. The image variance is derived from all pixels and represents variability at the scale of the individual pixel. The assumption here is, over the extensive study area, misregistration noise is the predominant influence on the variance of image differences, rather than actual land-use/land-cover changes (Gong et al., 1992; Verbyla & Boles, 2000).

To substantiate whether the compensation model reduced artifacts due to misregistration, we also compared local variance statistics for difference images derived from simple differencing and the compensation model. Fig. 8 is a graph of the mean values of local variance calculated for window sizes of 3×3, 5×5, 7×7, and 9×9 for simple difference and compensation model images of the extensive study area. As was the case for the global variance, the image mean of local variances of ΔNDVI for all three window sizes is lower for the products generated from the compensation model, comparable for ΔCh1 and higher for ΔCh4 (except for the 3×3 window size). This provides further evidence that the model reduced spurious changes from misregistration. Semi-variograms (not shown) followed the same relative trends as the global and local variance statistics for the simple difference and compensation model results (Dai & Khorram, 1997).

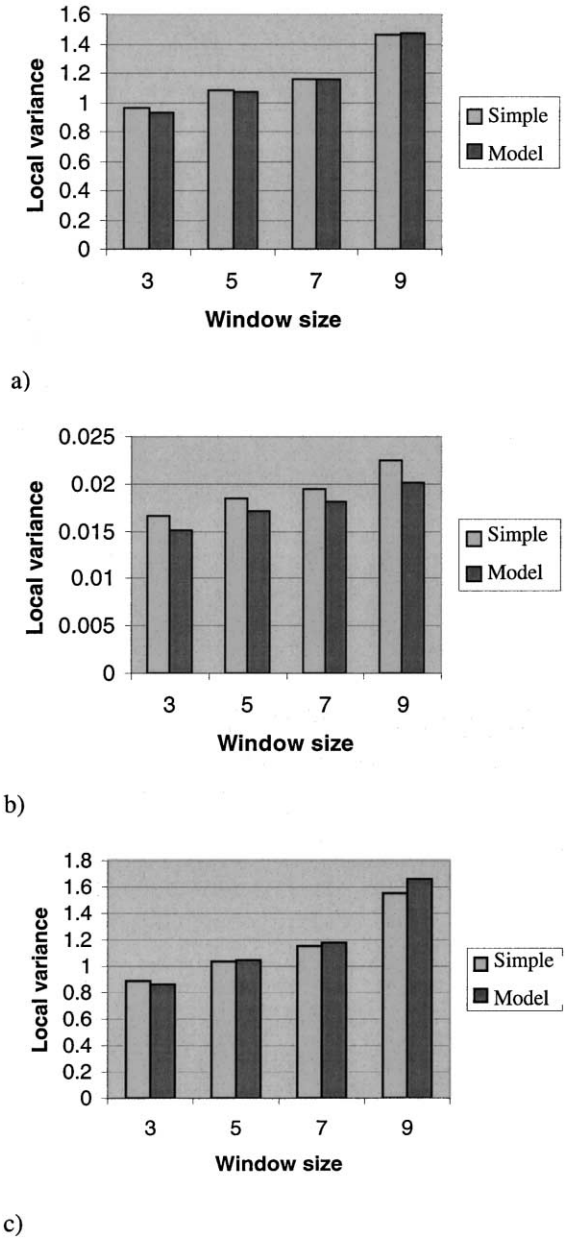

Fig. 8. Local variance statistics for products from simple image difference (Simple) and misregistration compensation model (Model); (a) ΔCh1, (b) ΔNDVI, and (c) ΔCh4. Reduction in local variance by the compensation model is attributed to reduction in artifacts in image differencing associated with misregistration.

6. Discussion and conclusions

6.1. Sensitivity to land-use/land-cover change

In spite of the large amount of land-use/land-cover change in the intensive study area during the 1990–1995 period, only two of the nearly 10,000 km^2 AVHRR pixels contained 100% land-use/land-cover change. Four pixels represented over 90% change and 10 over 80% change. Even large contiguous areas where natural vegetation cover converted to agriculture or was urbanized were depicted as multiple contiguous pixels with fractional amounts of land-use/land-cover change.

The strongest signals of temporal brightness change occurred for NDVI and Ch4 surface temperature products. The land-use/land-cover transition types with the most definitive AVHRR signals were "undeveloped to urban" and "undeveloped to water." Coastal sage scrub vegetation that is dominant in the most dynamically urbanizing portions of the study area has a low leaf area index (LAI) and high amounts of woody plant, litter, and bare soils cover. Thus, NDVI values are relatively low and surface temperature relatively high for this type of shrubland, compared to vegetation in more mesic landscapes. Transitions from this "undeveloped" shrubland land-use/land-cover type, with its sparse natural vegetation and high bare soil cover, to "urban" or "agricultural" types that contain irrigated green vegetation (e.g., grass lawns or crops) result in detectable increases in NDVI and decreases in Ch4 temperature. These findings should not necessarily be generalized to other parts of the world, but are likely to be similar to other semiarid

regions. Many of the rapidly urbanizing areas of the earth are in semiarid regions.

Besides that most of the land-use/land-cover changes are smaller in extent than the ground resolution element of AVHRR (Foody & Boyd, 1999), another factor explaining the low correlation between the amount of land-use/land-cover change and magnitude of AVHRR temporal differences is the juxtaposition of multiple types of transition sequences with varying image change signatures. Many AVHRR pixels for the San Diego County study area contained multiple polygons of differing land-use/land-cover change transition states. In several cases, the signs of the image difference signatures associated with different transitions were opposite.

Thus, we conclude that the 1-km (and larger) spatial resolution of AVHRR is too coarse to capture most land-use/land-cover change features of an urbanizing, semiarid region. Change detection products from TERRA MODIS imagery that are based on 0.25-km image data for visible and near infrared bands will likely be more sensitive to capturing such change features. At this finer spatial resolution, the likelihood is greater that more pixels will contain a larger fraction of a single land-use/land-cover transition type.

6.2. Misregistration effects and compensation

The basis for estimating misregistration fields was residual error data of GCPs selected from a library of control points that are utilized in the ADAPS registration processing of AVHRR data. The surfacing of GCP errors and subsequent subtraction of surfaces provides a convenient means for estimating the spatial distribution of misregistration, since the residual errors are reported upon completion of the ADAPS geometric processing. Alternative approaches to estimating GCP error would involve manual selection of ground test points (GTPs) or automated matching using image correlation techniques (Fonseca & Manjunath, 1996). Either approach will entail additional processing costs. The advantage of the compensation model is that neither geometric transformation nor subsequent resampling of the images would be required.

The magnitude of apparent errors and continuity of the misregistration fields derived from the AVHRR data set were encouraging, though the sparseness of GCPs is a concern. Errors for all GCPs in the extensive study area were subpixel in magnitude, with means of 0.23 and 0.18 pixel units in the x and y directions, respectively. These misregistration values are less than the more comprehensive estimates of AVHRR time series made by Meyer (1996), as our estimates are limited to near-nadir portions of the two specific AVHRR segments. For the most part, the misregistration fields were smoothly continuous. In a few instances, interpolation of GCPs associated with coastline features yielded abrupt discontinuities in the fields, but these artifacts were not extensive. With a density of around one GCP per 8800 km^2 (or one per 8800 pixels) for the land portion of the extensive area, misregistration fields derived from a relatively low density of GCPs should be considered approximations to the actual error surfaces.

While misregistration errors are apparently minimal, the mean values of MNEΔB of 0.02, 0.02, and 1.96 K for ΔCh1, ΔNDVI, and ΔCh4, respectively, imply that the combined effect of misregistration and local spatial brightness gradients can be substantial. Since large values of MNEΔB occur when high spatial gradients of brightness coincide with zones of higher magnitude misregistration error, they tended to occur at land–water interfaces, or the boundaries between agricultural, urban, and undeveloped land-use/land-cover types.

We propose the signal–noise ratio (S/MNEΔB) as an indicator of the detectability of particular transition sequences of land-use/land-cover change relative to misregistration effects. Signals (S) may be estimated by calculating differences of characteristic signatures of the beginning or end states of a particular transition sequence, for a given band or index (Stow et al., 1996). Signatures may be extracted from training sites that represent the initial state of land-use/land-cover transition from the first date and from training sites of the terminal state for the second date of imagery.

Results from testing the misregistration compensation model are encouraging, but not sufficiently conclusive to warrant usage without further testing and refinement. The keys to successful implementation are efficient and accurate derivation of misregistration fields and reliable estimates of spatial brightness gradients (($\Delta B/\Delta x$) and ($\Delta B/\Delta y$)). An improvement was the use of directional (forward or backwards) difference operators to estimate brightness gradients, rather than the central difference operator that was originally tested by Stow (1999). While the directional operator is a first-order and central difference operator a second-order approximation to a first derivative (Stow, 1987), the directional operator has the advantage of utilizing information on the sign of misregistration to estimate spatial gradients in the specific direction of the misregistration effect. However, if the magnitudes of misregistration were to be consistently greater than one pixel and spatial gradients were heterogeneous, either type of difference operator could be a poor estimator of ($\Delta B/\Delta x$) and ($\Delta B/\Delta y$) of the actual misregistration effect. Our results suggest that this is not the case for AVHRR data subjected to ADAPS geometric processing, nor should it be for multitemporal data sets from other moderate-to coarse-resolution satellite systems.

TERRA MODIS imagery would appear to be the most suitable candidate for testing, refining, and implementing the misregistration compensation model for improving land-use/land-cover change products. Similar to the ADAPS for AVHRR, an image-to-image registration routine is reported to be utilized in the MODIS processing sequence, which may provide a convenient source of information on relative registration errors between dates of MODIS imagery (Nishihama et al., 1997).

Acknowledgments

Brad Reed, Carolyn Gaeke, Jeff Eidenshink, and David Meyer of the USGS EROS Data Center provided valuable advice and metadata for NOAA AVHRR data used in this study.

References

Bastin, G. N., Pickup, G., & Pearce, G. (1995). Utility of AVHRR data for land degradation assessment: a case study. *International Journal of Remote Sensing*, *16*, 651–672.

Carmel, Y., Dean, D., & Flather, C. (2001). Combining location and classification error sources for estimating multi-temporal database accuracy. *Photogrammetric Engineering and Remote Sensing*, *67*, 865–873.

Cherchali, S., Amram, O., & Flouzat, G. (2000). Retrieval of temporal profiles of reflectances from simulated and real NOAA-AVHRR data over heterogeneous landscapes. *International Journal of Remote Sensing*, *21*, 753–775.

Coppin, P. R., & Bauer, M. E. (1996). Digital change detection in forest ecosystems with remote sensing imagery. *Remote Sensing Reviews*, *13*, 207–234.

Dai, X., & Khorram, S. (1997). Quantification of the impact of misregistration on the accuracy of remotely sensed change detection. In: Proceedings of the IEEE Geosciences and Remote Sensing Symposium (Texas, IEEE). (pp. 1763–1765).

Dai, X., & Khorram, S. (1998). SAR and InSAR—the effects of image misregistration on the accuracy of remotely sensed change detection. *IEEE Transactions on Geoscience and Remote Sensing*, *36*, 1566–1589.

Douglas, I. (1994). Human setllements. In: W. B. Meyer, & B. L. Turner II (Eds.), *Changes in land use and land cover: a global perspective* (pp. 149–169). Cambridge, UK: Cambridge Press.

Dozier, J. (1981). A method for satellite identification of surface temperature fields of sub-pixel resolution. *Remote Sensing of Environment*, *11*, 221–229.

Eidenshink, J. C. (1992). The 1990 conterminous U.S. AVHRR data set. *Photogrammetric Engineering and Remote Sensing*, *58*, 809–813.

Fonseca, L. M. G., & Manjunath, B. S. (1996). Registration techniques for multisensor remotely sensed imagery. *Photogrammetric Engineering and Remote Sensing*, *62*, 1049–1056.

Foody, G. M., & Boyd, D. S. (1999). Detection of partial land cover change associated with the migration of inter-class transitional zones. *International Journal of Remote Sensing*, *14*, 2723–2740.

Gong, P., LeDrew, E. F., & Miller, J. R. (1992). Registration–noise reduction in difference images for change detection. *International Journal of Remote Sensing*, *13*, 773–779.

Hope, A., Coulter, L., & Stow, D. (1999). Estimating lake area in an arctic landscape using linear mixture modelling with AVHRR data. *International Journal of Remote Sensing*, *20*, 829–835.

Lambin, E. F. (1997). Modelling and monitoring land-cover change processes in tropical regions. *Physical Geography*, *21*, 375–393.

Lambin, E. F., & Strahler, A. H. (1994). Indicators of land-cover change for change-vector analysis in multitemporal space at coarse spatial scales. *International Journal of Remote Sensing*, *15*, 2099–2119.

Malingreau, J. P. (1986). Global vegetation dynamics: satellite observations over Asia. *International Journal of Remote Sensing*, *7*, 1121–1146.

Meyer, D. J. (1996). Estimating the effective spatial resolution of AVHRR time series. *International Journal of Remote Sensing*, *17*, 2971–2980.

Mucher, C., Steinnnocher, K., Kressler, F., & Heunks, C. (2000). Land cover characterization and change detection for environmental monitoring of pan-Europe. *International Journal of Remote Sensing*, *21*, 1159–1181.

Nicholson, S. E., Tucker, C. J., & Ba, M. M. (1998). Desertification, drought and surface vegetation: an example from the West African Sahel. *Bulletin of the American Meteorological Society*, *79*, 815–829.

Nishihama, M., Wolfe, R., Solomon, D., Patt, F., Blanchette, J., Fleig, A., & Masuoka, E. (1997). MODIS Level 1A Earth Location Version 3.0. NASA Technical Memorandum SDST-092, NASA Goddard Space Flight Center.

Penner, J. E. (1994). Atmospheric chemistry and air quality. In: W. B. Meyer, & B. L. Turner II (Eds.), *Changes in land use and land cover: a global perspective* (pp. 175–210). Cambridge, UK: Cambridge Press.

Roy, D. (2000). The impact of misregistration upon composited wide field of view satellite data and implications for change. *IEEE Transactions on Geoscience and Remote Sensing*, *38*, 2017–2033.

Schultz, P. A., & Halpert, M. S. (1995). Global analysis of the relationships among a vegetation index, precipitation and land surface temperature. *International Journal of Remote Sensing*, *16*, 2755–2777.

Stow, D. (1999). Reducing misregistration effects for pixel-level analysis of land-cover change. *International Journal of Remote Sensing*, *20*, 2477–2483.

Stow, D., Hope, A., Nguyen, A., Phinn, S., & Benkelman, C. (1996). Monitoring detailed land surface changes from an airborne multispectral digital camera system. *IEEE Transactions on Geoscience and Remote Sensing*, *34*, 1191–1202.

Stow, D. A. (1987). Numerical derivation of a hydrodynamic surface flow field from time sequential remotely sensed data. *Remote Sensing of Environment*, *23*, 1–22.

Strahler, A. H., Woodcock, C. E., & Smith, J. A. (1986). On the nature of models in remote sensing. *Remote Sensing of Environment*, *20*, 121–139.

Townshend, J. R. G., Justice, C. O., Gurney, C., & McManus, J. (1992). The impact of misregistration on change detection. *IEEE Transactions on Geoscience and Remote Sensing*, *30*, 1054–1060.

Tucker, C. J., Dregne, H. D., & Newcomb, W. W. (1991). Expansion and contraction of the Sahara desert from 1908 to 1990. *Science*, *253*, 299–301.

Turner II, B. L., Meyer, W. B., & Skole, D. L. (1994). Global land-use/land-cover change: towards an integrated study. *Ambio*, *23*, 91–95.

Verbyla, D. L., & Boles, S. H. (2000). Bias in land cover change estimates due to misregistration. *International Journal of Remote Sensing*, *21*, 3553–3560.

Vitousek, P. (1994). Beyond global warming: ecology and global change. *Ecology*, *75*, 1861–1876.